

Charge-dependent model for many-body polarization, exchange, and dispersion interactions in hybrid quantum mechanical/molecular mechanical calculations

Timothy J. Giese and Darrin M. York^{a)}

Department of Chemistry, University of Minnesota Minneapolis, Minnesota 55455, USA

(Received 2 July 2007; accepted 7 August 2007; published online 15 November 2007)

This work explores a new charge-dependent energy model consisting of van der Waals and polarization interactions between the quantum mechanical (QM) and molecular mechanical (MM) regions in a combined QM/MM calculation. van der Waals interactions are commonly treated using empirical Lennard-Jones potentials, whose parameters are often chosen based on the QM atom type (e.g., based on hybridization or specific covalent bonding environment). This strategy for determination of QM/MM nonbonding interactions becomes tedious to parametrize and lacks robust transferability. Problems occur in the study of chemical reactions where the “atom type” is a complex function of the reaction coordinate. This is particularly problematic for reactions, where atoms or localized functional groups undergo changes in charge state and hybridization. In the present work we propose a new model for nonelectrostatic nonbonded interactions in QM/MM calculations that overcomes many of these problems. The model is based on a scaled overlap model for repulsive exchange and attractive dispersion interactions that is a function of atomic charge. The model is chemically significant since it properly correlates atomic size, softness, polarizability, and dispersion terms with minimal one-body parameters that are functions of the atomic charge. Tests of the model are examined for rare-gas interactions with neutral and charged atoms in order to demonstrate improved transferability. The present work provides a new framework for modeling QM/MM interactions with improved accuracy and transferability. © 2007 American Institute of Physics. [DOI: 10.1063/1.2778428]

I. INTRODUCTION

The development of improved methods for modeling chemical reactions that occur in complex biochemical environments is of considerable interest to the scientific community. Of particular importance are quantum mechanical (QM)/molecular mechanical (MM) methods^{1–5} that treat part of the system quantum mechanically and part with a molecular mechanical force field. These methods have been applied successfully to a host of problems involving chemical reaction mechanisms in solution,^{6,7} enzymes^{4,8} and ribozymes,⁹ the calculation of pK_a values,^{10,11} kinetic isotope effects,^{12–14} and ligand binding conformations and free energies.^{15,16} Recent advances in QM/MM modeling include the use of *ab initio* QM models in simulations,^{17–21} the development of fast semiempirical QM models with improved accuracy,^{22–38} QM/MM free-energy perturbation methods,^{16,39–43} treatment of excited states,^{44–48} quantum tunneling^{14,49–51} and concerted proton-electron transfers,^{52–56} integration with polarizable force field models,^{47,57} enhanced sampling techniques,⁵⁸ linear-scaling electrostatic algorithms^{33,59} and new solvation,^{60,61} charge scaling^{62,63} variational electrostatic projection,⁶⁴ and generalized solvent boundary potential methods.⁶⁵ The QM/MM methods serve as powerful tools in the arsenal of computational methods for biochemical mod-

eling. Nonetheless, applications of current state-of-the-art QM/MM methods have not been realized by the larger community, and currently there exists no general QM/MM model that is sufficiently reliable to be applied to a wide range of biocatalysis problems. One of the contributing factors to this limitation can be traced to the form of the QM/MM interaction. These and other factors severely limit the scope of applications that can be addressed by modern QM/MM methods, and largely restrict the user base to the realm of the specialist.

The most commonly applied QM/MM methods utilize a quantum mechanical model combined with an empirical force field where the QM/MM interaction energy consists of electrostatic, bonded, and nonbonded coupling elements. The electrostatic interaction term involves explicit QM coupling of the classical electrostatic potential of the MM system that enters directly into the quantum Hamiltonian as an external potential. The so-called “bonded” interaction is used when division of the QM and MM subsystems occurs across a chemical bond, in which case one of several specialized techniques are used in order to cap the quantum system and prevent the boundary from having problems associated with charge normalization of dangling bond character.^{2,66–74} The nonbonded interaction is most frequently modeled as a simple empirical van der Waals interaction such as a Lennard-Jones 6–12 potential. This term is purely empirical and completely neglects explicit coupling to the quantum mechanical electronic degrees of freedom.

^{a)}Author to whom correspondence should be addressed. Electronic mail: york@chem.umn.edu

Many-body polarization and exchange effects are intimately coupled.⁷⁵ The lack of explicit quantum mechanical coupling of the van der Waals QM/MM interaction energy is at the root of many problems in QM/MM modeling. In molecular mechanical force fields, van der Waals parameters are typically assigned based on the concept of an *atom type*.^{76,77} An atom type is a construct that allows atoms in similar chemical environments to be assigned the same force field parameters. This is a reasonable strategy for many problems where it is sufficient to use a molecular mechanical force field where the charge state and chemical bonding environment remains fixed. However, in the case of QM/MM calculations, atoms may undergo considerable changes in charge state and chemical bonding environment as a function of the reaction coordinate or perturbation parameter. In the case of reactions that involve highly charged species, such as phosphate hydrolysis and phosphoryl transfer reactions,^{78–80} the solvent effect is tremendously sensitive to the van der Waals radii that dictate the degree to which solvent can approach ionic substates.

As an example, in a phosphate hydrolysis reaction, an oxygen that is part of a solvent water molecule might become an activated hydroxide ion that then goes on to attack a phosphate, ultimately transferring a proton and becoming a nonbridging phosphoryl oxygen. No single set of van der Waals parameters can reliably reproduce nonbonded interactions across such a diverse set of charge states and chemical bonding environments. Much effort must be spent in tuning van der Waals parameters to obtain reasonable average values for specific reactions of interest.^{81–84} This limits the robustness, transferability, and range of applicability of QM/MM models and their use as a predictive tool to study biocatalysis.

The present work describes a new model for nonbonded QM/MM interactions that is explicitly coupled to the QM electron density. The method is based on a charge-dependent density overlap model for exchange and dispersion interactions, integrated with a charge-dependent polarization response reported previously. The model is physically realistic in the sense that the magnitude of the exchange repulsion and dispersion increases with increasing negative charge, and in a manner consistent with trends in atomic size and polarizability. In this way, the conventional nonbonded van der Waals component of the QM/MM interaction that relies on predetermined atom type parameters, which are independent of charge state, is replaced by one-body *atom* parameters that adjust appropriately as a function of charge state. The model is tested against new high-level benchmark quantum data for nonbonded interactions of rare gases with atoms in different charge states. Results demonstrate that the model is able to account charge dependence of the nonbonded interaction energy curves significantly better than the widely used static Lennard-Jones model. The outline of the paper is as follows. Section II describes the computational methods, and Sec. III presents and discusses key results for nonbonded interactions for different atoms and ions. Section IV concludes with a summary of the key results and outline of directions for future research.

II. METHODS

This section describes the QM/MM models. In the following, we outline the functional form of the new charge-dependent models. In doing so, we emphasize those terms that have explicit charge dependence by giving them functional arguments (indicated in brackets) or function arguments (indicated in parentheses).

A. Combined QM/MM potential

The total energy of a QM/MM calculation is decomposed into self-consistent field (SCF), post-SCF, and MM components

$$E[\rho, \mathbf{q}] = E_{\text{SCF}}[\rho, \mathbf{q}] + E_{\text{post-SCF}}[\rho, \mathbf{q}] + E_{\text{MM}}[\mathbf{q}], \quad (1)$$

where $\rho(\mathbf{r})$ is the QM electron density, i.e.,

$$\rho(\mathbf{r}) = \langle \mathbf{r} | \hat{\rho} | \mathbf{r} \rangle = \sum_i n_i |\psi(\mathbf{r})|^2. \quad (2)$$

\mathbf{q} is the *static* charge density of the MM region, and $E_{\text{MM}}[\mathbf{q}]$ describes the MM-MM interactions. The SCF energy is the energy expectation value of the QM region in the field of the external MM point charges

$$E_{\text{SCF}}[\rho, \mathbf{q}] = \langle \Psi | \hat{H}_{\text{QM}} - \sum_{i \in \text{MM}} \frac{q_i}{|\mathbf{r} - \mathbf{R}_i|} | \Psi \rangle, \quad (3)$$

where \hat{H}_{QM} is the quantum mechanical Hamiltonian. The modified neglect of differential overlap with *d*-orbital extension (MNDO)/d Hamiltonian⁸⁵ is considered in the present work because we have previously published⁸⁶ polarization correction (discussed below) parameters for this Hamiltonian; however, it is stressed that the equations described hereto do not assume a specific form of \hat{H}_{QM} .

The SCF energy is variationally optimized with respect to the electronic degrees of freedom (i.e., orbital coefficients in this case) to yield a converged wave function and corresponding SCF density in Eq. (2). The SCF density is then used in a post-SCF correction, which consists of charge-dependent density response based on chemical potential equalization^{86,87} (CPE) and charge-dependent QM/MM van der Waals components

$$E_{\text{post-SCF}}[\rho, \mathbf{q}] = E_{\text{CPE}}[\rho, \mathbf{q}] + E_{\text{vdW}}[\rho, \mathbf{q}], \quad (4)$$

which are discussed in Secs. II B and II C, respectively. The net interaction energy, $\Delta E[\rho, \mathbf{q}]$, between the QM and MM systems is given by

$$\begin{aligned} \Delta E[\rho, \mathbf{q}] &= E[\rho, \mathbf{q}] - E[\rho_0, 0] - E[0, \mathbf{q}] \\ &= (E_{\text{SCF}}[\rho, \mathbf{q}] - E_{\text{SCF}}[\rho_0, 0]) \\ &\quad + (E_{\text{CPE}}[\rho, \mathbf{q}] - E_{\text{CPE}}[\rho_0, 0] - E_{\text{CPE}}[0, \mathbf{q}]) \\ &\quad + E_{\text{vdW}}[\rho, \mathbf{q}], \end{aligned} \quad (5)$$

where ρ_0 is the SCF density in the absence of the MM field and ρ is the SCF density in the presence of the MM field. Note that $E_{\text{MM}}[\mathbf{q}]$ represents a static MM energy and therefore drops from the expression for the QM/MM interaction energy. The systems considered in this work consist of a

polarizable rare gas MM probe with zero charge interacting with an isolated QM atom *or atomic ion*. For these specific cases, Eq. (5) reduces to

$$\Delta E[\rho, \mathbf{q}] = E_{\text{CPE}}[\rho, \mathbf{q}] + E_{\text{vdW}}[\rho, \mathbf{q}] = E_{\text{post-SCF}}[\rho, \mathbf{q}]. \quad (6)$$

For clarity we note that, for the systems studied in the present work, $E_{\text{CPE}}[\rho, \mathbf{q}]$ is nonzero if the QM region is an atomic ion, and zero when the QM region is an isolated atom.

B. Charge-dependent polarization correction

Charge-dependent polarization⁸⁶ is modeled by a CPE-correction term, $E_{\text{CPE}}[\rho, \mathbf{q}]$. In the present work, a charge-dependent CPE response is used to model proper polarization response of both the QM atoms⁸⁶ and the MM atoms, in a manner similar to the original formulation of the method⁸⁷ but extended in this work to be a function of charge.

The response density is represented by an auxiliary basis of atom-centered (both QM *and* MM) Gaussian dipole functions, $\varphi_i(\mathbf{r})$,

$$m_i = \begin{cases} \int \left(\sum_{j \in \text{QM}} D_{ij}(r_{ij}) \phi_j(\mathbf{r}) - \sum_{j \in \text{MM}} q_j / |\mathbf{r} - \mathbf{R}_j| \right) \varphi_i(\mathbf{r}) d^3r & \text{if } i \in \text{QM} \\ \int \left(\sum_{j \in \text{QM}} \phi_j(\mathbf{r}) - \sum_{j \in \text{MM}}^* q_j / |\mathbf{r} - \mathbf{R}_j| \right) \varphi_i(\mathbf{r}) d^3r & \text{if } i \in \text{MM} \end{cases} \quad (10)$$

and

$$\eta_{ij} = D_{ij}(r_{ij}) \iint \frac{\varphi_i(\mathbf{r}) \varphi_j(\mathbf{r}')}{|\mathbf{r} - \mathbf{r}'|} d^3r d^3r'. \quad (11)$$

$\sum_{j \in \text{MM}}^*$ is a restricted summation that includes the *nonbonded* MM-MM interactions. The Coulomb approximation to the universal functional is similarly insufficient to describe density response between analogously arranged, bonded-type configurations of QM atoms. Therefore, the short-ranged QM-QM interactions are damped by $D_{ij}(r_{ij})$ [see Eq. (18) in Ref. 86]; however, in this work, both the MM region and the QM region consist of a single atom or ion, i.e., all interactions are nonbonded and thus, $D_{ij}(r_{ij})=1$. $\phi_j(\mathbf{r})$ is the electrostatic potential of the Mulliken partitioned QM charge and dipole moment of QM atom j .

The response coefficients of the CPE correction are obtained from a variational optimization of the response density (provided a *fixed* reference density) and results in a linear solution

$$\mathbf{c} = -\boldsymbol{\eta}^{-1} \cdot \mathbf{m}. \quad (12)$$

$$\begin{aligned} \delta\rho(\mathbf{r}) &= \sum_i c_i \varphi_i(\mathbf{r}) \\ &= \sum_i c_i 2\xi_i(q_i)^2 \left(\frac{\xi_i(q_i)^2}{\pi} \right)^{3/2} (u - U_i) e^{-\xi_i(q_i)^2 |\mathbf{r} - \mathbf{R}_i|^2}, \end{aligned} \quad (7)$$

where u and U_i are the x , y , or z components of \mathbf{r} and \mathbf{R}_i , respectively, and $\xi_i(q_i)$ is the Gaussian exponent, which explicitly depends on the static charge (MM) or the SCF Mulliken charge (QM) of the atom through the relation⁸⁶

$$\xi_i(q_i) = \left(\frac{3}{\Delta\alpha_i(0)} \sqrt{\frac{\pi}{2}} \right)^{1/3} e^{B_i q_i}, \quad (8)$$

where $\Delta\alpha_i(0)$ is the polarizability *correction* to the neutral atom and B_i is a parameter describing the change in atom polarizability as a function of its charge.

By performing a Taylor series expansion of the density functional about the SCF density to second order in the density response, and subsequent projection of the response density into a basis, a matrix formulation of the response energy is obtained,

$$E_{\text{CPE}}[\rho, \mathbf{q}] = \mathbf{c}^T \cdot \mathbf{m} + \frac{1}{2} \mathbf{c}^T \cdot \boldsymbol{\eta} \cdot \mathbf{c}, \quad (9)$$

where

C. Charge-dependent van der Waals correction

The charge-dependent QM/MM van der Waals correction is decomposed into a summation over pairwise repulsive $E_{\text{rep},ij}$ and dispersion $E_{\text{disp},ij}$ potentials

$$\begin{aligned} E_{\text{vdW}}[\rho, \mathbf{q}] &= \sum_{i \in \text{QM}} \sum_{j \in \text{MM}} E_{\text{rep},ij}[r_{ij}, q_i(\rho), q_j] \\ &\quad + E_{\text{disp},ij}[r_{ij}, q_i(\rho), q_j], \end{aligned} \quad (13)$$

where $q_i(\rho)$ is the Mulliken partitioned partial charge of QM atom i and q_j is the static MM charge of atom j . The forms of $E_{\text{rep},ij}$ and $E_{\text{disp},ij}$ are described in Secs. II C 1 and II C 2, respectively.

1. Repulsive potential

It has previously been recognized that intermolecular repulsion energy is approximately related to the overlap between unperturbed charge densities,⁸⁸⁻⁹⁰

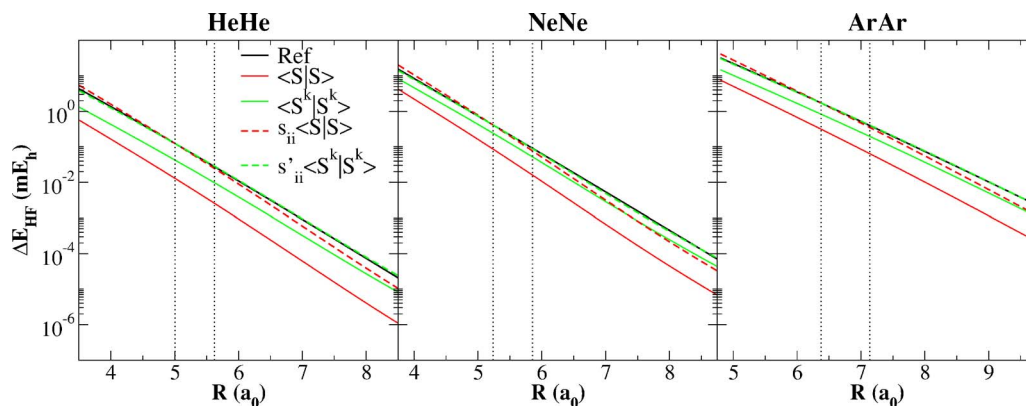


FIG. 1. (Color online) Comparison between nonbonded van der Waals repulsion models. $s_{ii}\langle S|S\rangle$ and $s'_{ii}\langle S^k|S^k\rangle$ correspond to Eqs. (14) and (15), respectively, and *Ref.* is the high-level HF potential from Ref. 91. The unperturbed atomic densities were computed at HF/aug-cc-pV5Z.

$$E_{\text{rep},ij}(r_{ij}) \approx s_{ij} \int \rho_i(\mathbf{r} - \mathbf{R}_i) \rho_j(\mathbf{r} - \mathbf{R}_j) d^3r, \quad (14)$$

where s_{ij} is a constant. It is worthwhile to consider, briefly, how to approach the mathematical modeling of Eq. (14). First, given accurate atomic densities, the overlap integral can be solved via numerical quadrature; however, a computationally inexpensive approach is desirable. One could represent the result of the overlap integral as a spline function, however, it will become advantageous to compute the overlap integral for various charge states, and it is not obvious how one would accommodate charge dependence with a spline function corresponding to specific charge states or generate the spline for fractionally charged atoms. Last, it should be emphasized that Eq. (14) is an approximation and there is no guarantee that a better model of electron density would necessarily yield a better description of repulsion. We have empirically observed that the Hartree-Fock energy between Rg-X , where $\text{Rg} \in (\text{He}, \text{Ne}, \text{Ar})$ and $\text{X} \in (\text{He}, \text{Ne}, \text{Ar}, \text{F}, \text{Cl})$, can be alternatively modeled by

$$E_{\text{rep},ij}(r_{ij}) \approx s_{ij} \int \rho_i(\mathbf{r} - \mathbf{R}_i)^k \rho_j(\mathbf{r} - \mathbf{R}_j)^k d^3r, \quad (15)$$

where k is a parameter, which we empirically observed to be 0.92. Figure 1 compares Eqs. (14) and (15) using Hartree-Fock (HF)/aug-cc-pV5Z atomic densities against the accurate HF potential in Ref. 91.

The model explored in this work relates the repulsion energy to the overlap between Slater monopole functions, i.e.,

$$\begin{aligned} E_{\text{rep},ij}(r_{ij}, q_i, q_j) &= s_i s_j \int \frac{\zeta_i(q_i)^3}{8\pi} e^{-\zeta_i(q_i)|\mathbf{r}-\mathbf{R}_i|} \frac{\zeta_j(q_j)^3}{8\pi} e^{-\zeta_j(q_j)|\mathbf{r}-\mathbf{R}_j|} d^3r \\ &= s_i s_j \langle S_i | S_j \rangle, \end{aligned} \quad (16)$$

where s_i and s_j are one-body parameters and the ζ exponents explicitly depend on the atomic charge through the empirical relation

$$\zeta_i(q_i) = \zeta_i(0) e^{\zeta_{q,i} q_i}. \quad (17)$$

The normalized Slater monopole overlap is

$$\langle S_i | S_j \rangle = \zeta_{ij} (\Delta_{ij} - \Delta_{ji}), \quad (18)$$

where

$$\zeta_{ij} = \frac{\zeta_i(q_i)^3 \zeta_j(q_j)^3}{8\pi [\zeta_i(q_i)^2 - \zeta_j(q_j)^2]^3} \quad (19)$$

and

$$\Delta_{ij} = \frac{\zeta_j(q_j) e^{-\zeta_i(q_i) r_{ij}}}{r_{ij}} \{4\zeta_i(q_i) + r_{ij} [\zeta_i(q_i)^2 - \zeta_j(q_j)^2]\}. \quad (20)$$

Numerical instabilities are avoided in the cases where $\zeta_i(q_i) \approx \zeta_j(q_j)$ and/or $r_{ij} \approx 0$ by evaluating the appropriate limit(s).

Equation (17) uses a single parameter to describe the charge dependence of the Slater ζ exponent, $\zeta_{q,i}$. An exponential form for the charge dependence was chosen to ensure that $\zeta_i(q_i)$ is a positive monotonic function whose derivative is a negative function ($\zeta_{q,i} < 0$). These mathematical constraints arise from three very simple physical arguments: (1) $\zeta_i(q_i)$ should never equal zero because the overlap of two such functions would be independent of separation. Therefore, $\zeta_i(q_i)$ must be either a positive or negative function. (2) $\zeta_i(q_i)$ must be monotonic because there is no local extrema in atomic size as a function of charge. (3) $\zeta_i(q_i)$ must be a positive function with negative derivative because anions are larger and more diffuse than cations.

The $\zeta_i(0)$ parameters were initially parametrized to reproduce the overlap between unperturbed densities of homonuclear dimers; however, better agreement with *ab initio* potentials was possible by scaling $\zeta_i(0)$ by a factor of 0.92, i.e., the k parameter [Eq. (15)] is effectively treated by the scaling of the $\zeta_i(0)$ parameters.

2. Dispersion potential

The charge-dependent pairwise dispersion potential is the familiar damped multipole expansion

$$E_{\text{disp},ij}(r_{ij},q_i,q_j) = - \sum_{n=3}^4 S_{2n}(r_{ij},b_{ij}) \frac{C_{2n,ij}(q_i,q_j)}{r_{ij}^{2n}}, \quad (21)$$

where $C_{2n,ij}(q_i,q_j)$ is a charge-dependent dispersion coefficient and $S_{2n}(r_{ij},b_{ij})$ is the Tang-Toennies (TT) damping function.⁹²

The charge dependent C_6 and C_8 terms are computed from the expressions developed by Pellenq and Nicholson^{93,94} (PN), which do *not* contain any pairwise parameters. The expressions are

$$C_{6,ij}(q_i,q_j) = \frac{3}{2} \frac{\eta_{1,i}\eta_{1,j}}{\eta_{1,i} + \eta_{1,j}} \alpha_{1,i}(q_i)\alpha_{1,j}(q_j) \quad (22)$$

and

$$C_{8,ij}(q_i,q_j) = \frac{15}{4} \left(\frac{\eta_{1,i}(q_i)\eta_{2,j}(q_j)}{\eta_{1,i}(q_i) + \eta_{2,j}(q_j)} \alpha_{1,i}(q_i)\alpha_{2,j} + \frac{\eta_{2,i}(q_i)\eta_{1,j}(q_j)}{\eta_{2,i}(q_i) + \eta_{1,j}(q_j)} \alpha_{2,i}\alpha_{1,j}(q_j) \right), \quad (23)$$

where $\alpha_{1,i}$ and $\alpha_{2,i}$ are the dipole and quadrupole polarizability of atom i , respectively, and $\eta_{1,i}$ and $\eta_{2,i}$ are formally related to l -pole transition energies, but have been shown to be well modeled by a parameter interpreted as the effective number of electrons,⁹³

$$\eta_{1,i}(q_i) = \sqrt{\frac{N_{\text{eff},i}(q_i)}{\alpha_{1,i}(q_i)}} \quad (24)$$

and

$$\eta_{2,i}(q_i) = \left(\frac{\sqrt{9N_{\text{eff},i}(q_i)\alpha_{1,i}(q_i)}}{\alpha_{2,i}} \right)^{1/2}. \quad (25)$$

$N_{\text{eff},i}(q_i)$ is explicitly a function of atomic charge and PN suggested⁹³ the form

$$N_{\text{eff},i}(q_i) = N_{\text{eff},i}(0) - q_i. \quad (26)$$

However, it should be noted that $N_{\text{eff},i}(0)$ is less than the number of valence electrons (see Table II in Ref. 93) and from Eqs. (24) and (25), clearly the condition $N_{\text{eff},i}(q_i) \geq 0$ for all q_i must hold. In order to satisfy the mathematical constraint without introducing new charge-dependence parameters, we suggest an alternate scaled form

$$N_{\text{eff},i}(q_i) = \begin{cases} N_{\text{val},i}(q_i)N_{\text{eff},i}(0)/N_{\text{val},i}(0) & \text{if } N_{\text{val},i}(q_i) > 0 \\ 0 & \text{if } N_{\text{val},i}(q_i) \leq 0, \end{cases} \quad (27)$$

where $N_{\text{val},i}(0)$ is the number of valence electrons on neutral atom i and

$$N_{\text{val},i}(q_i) = N_{\text{val},i}(0) - q_i. \quad (28)$$

Note that an atom's valence shell has been totally ionized when $N_{\text{eff},i}(q_i)=0$ and thus prevents the atom from contributing to the dispersion energy, i.e., this is a frozen-core-like approximation.

Based on the work of Giese and York⁸⁶ the dipole polarizability is treated as an exponential function of charge

$$\alpha_{1,i}(q_i) = \alpha_{1,i}(0)e^{-3B_i q_i}. \quad (29)$$

Note that the parameter B_i appearing in Eqs. (8) and (29) are the same. In principle, the quadrupole and higher-order polarizability terms could also be made functions of charge; however, the C_6 term dominates the dispersive interaction, and in the present work, the inclusion of higher-order polarizability corrections was observed to be of negligible benefit. Similarly, the multipole expansion [Eq. (21)] could be carried out to C_{16} by using the expression for C_{10} given by PN (Ref. 93) and then approximating the higher-order coefficients using the relations derived by Thakker;⁹⁵ however, we have so far found it acceptable to truncate the expansion to C_8 and modify $\alpha_{2,i}$ as a parameter, when necessary.

The TT damping function is given by⁹²

$$S_{2n}(r_{ij},b_{ij}) = 1 - e^{-b_{ij}(r_{ij})r_{ij}} \sum_{k=0}^{2n} \frac{[b_{ij}(r_{ij})r_{ij}]^k}{k!}. \quad (30)$$

The b_{ij} parameter has traditionally been regarded as a pairwise constant corresponding to a Born-Mayer fit exponent to the repulsive potential; however, the definition was later revised for repulsive potentials not of pure exponential character,^{96,97}

$$b_{ij}(r_{ij}) = - \frac{d}{dr_{ij}} \ln E_{\text{rep},ij}(r_{ij},q_i,q_j) = \frac{1}{E_{\text{rep},ij}(r_{ij},q_i,q_j)} \frac{dE_{\text{rep},ij}(r_{ij},q_i,q_j)}{dr_{ij}}. \quad (31)$$

The expression used for $b_{ij}(r_{ij})$ is determined by inserting Eq. (16)

$$\frac{dE_{\text{rep},ij}(r_{ij},q_i,q_j)}{dr_{ij}} = s_i s_j \frac{d}{dr_{ij}} \langle S_i | S_j \rangle = s_i s_j \zeta_{ij} (\Delta'_{ij} - \Delta'_{ji}), \quad (32)$$

where

$$\Delta'_{ij} = \zeta_j(q_j) \frac{e^{-\zeta_i(q_i)r_{ij}}}{r_{ij}} [\zeta_i(q_i)^2 - \zeta_j(q_j)^2] - \Delta_{ij} \left(\frac{1}{r_{ij}} + \zeta_i(q_i) \right) \quad (33)$$

thus,

$$b_{ij}(r_{ij}) = \frac{\Delta'_{ij} - \Delta'_{ji}}{\Delta_{ij} - \Delta_{ji}}. \quad (34)$$

Note that $b_{ij}(r_{ij})$ is computed solely from 1-body parameters.

D. *Ab initio* reference data

The systems studied are all combinations of RgX where Rg \in (He, Ne, Ar) and X \in (He, Ne, Ar, F, F⁻, Cl, Cl⁻). All *ab initio* interaction energies in this work are corrected for basis set superposition error using the counterpoise method of Boys and Bernardi,⁹⁸

$$\Delta E(AB;AB) = E(AB;AB) - E(A;AB) - E(B;AB), \quad (35)$$

where $E(X;AB)$ is the energy of the system X in the basis of AB . Since all interaction energies referred to in this manuscript are counterpoise corrected, $\Delta E(AB;AB)$ will hence-

forth be denoted ΔE . The total interaction energy ΔE_{tot} is decomposed into Hartree-Fock self-consistent field (HF) and post-HF components,

$$\Delta E_{\text{tot}} = \Delta E_{\text{HF}}^{\text{cbs}} + \Delta \Delta E_{\text{post-HF}}, \quad (36)$$

where $\Delta \Delta E_{\text{post-HF}}$ is a complete basis set (cbs) extrapolated MP2 correlation energy with a CCSD(T)/aug-cc-pVTZ correlation correction, i.e.,

$$\Delta \Delta E_{\text{post-HF}} = \Delta \Delta E_{\text{MP2}}^{\text{cbs}} + (\Delta \Delta E_{\text{CCSD(T)}}^{\text{aTZ}} - \Delta \Delta E_{\text{MP2}}^{\text{aTZ}}), \quad (37)$$

where

$$\Delta \Delta E_{\text{MP2}}^{\text{aTZ}} = \Delta E_{\text{MP2}}^{\text{aTZ}} - \Delta E_{\text{HF}}^{\text{aTZ}}, \quad (38)$$

$$\Delta \Delta E_{\text{CCSD(T)}}^{\text{aTZ}} = \Delta E_{\text{CCSD(T)}}^{\text{aTZ}} - \Delta E_{\text{HF}}^{\text{aTZ}}. \quad (39)$$

Complete basis set extrapolated quantities are obtained from fitting the quantity to a function that depends on the cardinal index of the basis and extrapolating the parametrized function to its asymptotic value. In this work, the energies were computed using the aug-cc-pVDZ, aug-cc-pVTZ, and aug-cc-pVQZ basis sets^{99–101} (abbreviated throughout as aDZ, aTZ, and aQZ, respectively) and using the extrapolation form suggested by Woon and Dunning,¹⁰²

$$Q^{\text{aXZ}} = Q^{\text{cbs}} + Ae^{-(X-1)} + Be^{-(X-1)^2}, \quad (40)$$

where Q is the quantity being extrapolated (either ΔE_{HF} or $\Delta \Delta E_{\text{MP2}}$), X is the cardinal index of the basis, i.e., $X=2, 3$, and 4 for the basis sets aDZ, aTZ, and aQZ, respectively, and A and B are parameters also determined upon solving the set of simultaneous equations; however, the asymptotic value of the expression involves Q^{cbs} only.

The rare gas dimer potentials were taken from Ref. 91. The total interaction potential are counterpoise corrected CCSD(T)/aug-cc-pV5Z supplemented with a set of (3s3p2d2f1g) bond functions. The HF component of the total energy is the HF energy computed in the same basis, and the post-HF component is the difference between the total and HF interaction energies.

III. RESULTS AND DISCUSSION

Section III A examines the relationship between the repulsive Hartree-Fock interaction energy and atomic overlap as observed in rare gas dimers, which is used to motivate different parametric forms. Section III B presents the model parameters and describes the Nomenclature used in the remaining discussion. Sections III C and III D compare the current method with *ab initio* results and standard Lennard-Jones (LJ) models, and discusses the relative importance of the parameters within the current model.

A. Motivation of the functional form for the repulsive potential

Section II C 1 described an approximate relationship between the repulsive component of the van der Waals energy, $E_{\text{rep},ij}$, and atomic overlap, $\langle S_i | S_j \rangle$, [see Eqs. (14) and (15)]. In order to arrive at these functional forms, we investigated the repulsion energy between rare gas atoms as a function of

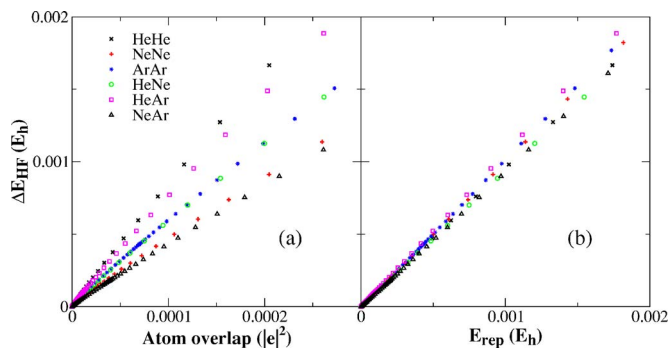


FIG. 2. (Color online) Approximate linear relationship between the repulsive HF interaction vs overlap between rare gas dimers (left) and model repulsive energy (right). The model repulsive energy is given by Eq. (16), and parameters are shown in Table I.

overlap. Figure 1 plots the *ab initio* Hartree-Fock interaction energy, ΔE_{HF} (plotted on a logarithmic scale) for HeHe, NeNe, and ArAr, as a function of interatomic separation, and compares it with $\langle S_i | S_j \rangle$ and the repulsion energy models Eqs. (14) and (15). The logarithm of ΔE_{HF} and $\langle S_i | S_j \rangle$ are nearly linear, as are the related models for $E_{\text{rep},ij}$; however, $\langle S_i | S_j \rangle$ is both shifted from, and has a different slope than, ΔE_{HF} . The shift in the atomic overlap model can be corrected by multiplication by a parameter constant (which is additive on the logarithm scale), as used in [Eq. (14)]. The slope of the resulting line, however, is still not well matched with ΔE_{HF} . This can be remedied by the nonlinear overlap model [Eq. (15)] which, in addition to a multiplicative prefactor, has an additional parameter that raises $\langle S_i | S_j \rangle$ by a noninteger power (designated k). Equation (15) accurately models ΔE_{HF} over the range 3.5–9.5 a.u. (1.9–5.0 Å). Note also that the nonlinear parameter, k in Eq. (15), has a value (0.92), which is close to unity and is transferable between different dimers.

The above discussion provides impetus for building a repulsion energy model motivated by Eq. (15) using a universal nonlinear scaling parameter $k=0.92$. We begin with the simplest possible functional form for the model repulsion energy given in Eq. (16). We follow a stepwise procedure, where first we consider the atomic overlap modeled as the overlap of two spherical Slater s functions located at the atomic centers. The Slater exponents are chosen to reproduce as closely as possible the interatomic overlap for the rare gas homodimer systems. The Slater exponents fit to the interatomic overlap were then scaled by k , in accord with Eq. (15), in order to arrive at the charge-independent Slater exponents [$\zeta_i(0)$ parameters in Eq. (17)]. With these Slater exponents, the one-body prefactors, s_i , in Eq. (16) were fit to the homodimer *ab initio* Hartree-Fock interaction energy curves. It was shown for the rare gas homodimers in Fig. 1 that the logarithms of the exchange repulsion energy and overlap are strongly correlated, and we observe also that there is significant correlation between repulsive energy and overlap for the rare gas heterodimers (Fig. 2, left). When Eq. (16) is used with the one-body parameters, a very good fit is obtained for both the homodimer and heterodimer energies (Fig. 2, right).

TABLE I. CPE+OPNQ parameters. All values given in a.u.

	He	Ne	Ar	F	Cl
$\zeta(0)$	2.780 04 ^a	2.795 06 ^a	2.155 06 ^a	2.75	2.15
ζ_q	0.0	0.0	0.0	-0.37	-0.26
s	4.1	10.0	20.1	7.2	16.1
$N_{\text{eff}}(0)$	1.509 8 ^b	3.690 1 ^b	5.306 2 ^b	4.086 ^b	5.551 ^b
α_1	1.359 6 ^b	2.668 9 ^b	11.083 9 ^b	3.759 ^b	14.71 ^b
α_2	2.334 1 ^b	7.963 4 ^b	120.0	0.0	81.79 ^b
$\Delta\alpha(0)$	1.359 6 ^c	2.668 9 ^c	11.083 9 ^c	3.596 45 ^d	8.113 32 ^c
B	0.0	0.0	0.0	0.222 86 ^d	0.300 45 ^c

^aOptimized directly to the homonuclear diatomic overlap integral of unperturbed densities obtained at HF/aug-cc-pV5Z and scaled by 0.92.

^bTaken from Refs. 93 and 94.

^cThe semiempirical implementation used in this study does not provide rare gases with orbital degrees of freedom and, therefore, the polarizability correction is defined as α_1 .

^dChosen to yield atom and ion polarizabilities listed in Ref. 104.

^eTaken from Ref. 86.

B. Determination of the model parameters

The charge-dependent model described in Sec. II will henceforth be denoted OPNQ, the parameters of which are given in Table I. A charge-independent variant of OPNQ, designated OPN, is also discussed to characterize the effect of the charge dependence of the model. The OPN model differs from OPNQ by removal of charge dependence only, i.e., $q_i=0$ when calculating $\zeta(q_i)$, $\xi(q_i)$, $\alpha_1(q_i)$, and $N_{\text{eff}}(q_i)$ from Eqs. (17), (8), (29), and (27), respectively.

The OPN rare gas parameters were chosen to reproduce the homonuclear dimer potentials, as described in Sec. III A. The OPN parameters for F and Cl atoms were obtained by fitting to the NeF and NeCl potential energy curves, respectively. The approach of fitting the F and Cl parameters to the Ne probe potential was chosen to address transferability through application to the He and Ar potentials. Transferability of the rare gas parameters are similarly examined in the heteronuclear rare gas potentials.

The OPNQ method introduces the charge dependence to the $\zeta(q_i)$, $\xi(q_i)$, $\alpha_1(q_i)$, and $N_{\text{eff}}(q_i)$ parameters and is, therefore, identical to OPN for neutral atom potentials, but greatly improves the potentials involving ions. The charge dependence of these parameters require the use of the ζ_q [Eq. (17)] and B [Eq. (29)] parameters. The ζ_q parameter for F and Cl were chosen to reproduce the NeF⁻ and ArF⁻ potentials, respectively, while fixing the B parameter [Eq. (29)] to that which reproduces atom and anion polarizabilities.

The OPN and OPNQ models are compared against the traditional LJ potential. The Lennard-Jones model is decomposed into repulsive r^{-12} and attractive r^{-6} components,

$$E_{\text{LJ},ij}(r_{ij}) = E_{\text{repLJ},ij}(r_{ij}) + E_{\text{dispLJ},ij}(r_{ij}), \quad (41)$$

where

$$E_{\text{repLJ},ij}(r_{ij}) = 4\epsilon_{ij} \left(\frac{\sigma_{ij}}{r_{ij}} \right)^{12} = \epsilon_{ij} \left(\frac{R_{e,ij}}{r_{ij}} \right)^{12} \quad (42)$$

and

$$E_{\text{dispLJ},ij}(r_{ij}) = -4\epsilon_{ij} \left(\frac{\sigma_{ij}}{r_{ij}} \right)^6 = -2\epsilon_{ij} \left(\frac{R_{e,ij}}{r_{ij}} \right)^6, \quad (43)$$

where ϵ_{ij} is the well depth at the minimum $R_{e,ij}$ [i.e., $E_{\text{LJ},ij}(R_{e,ij}) = -\epsilon_{ij}$] and σ_{ij} is the contact distance where the van der Waals dimer potential crosses zero [i.e., $E_{\text{LJ},ij}(\sigma_{ij}) = 0$]. The contact distance and minimum in the LJ model are not independent parameters, and are related by $R_{e,ij} = 2^{1/6}\sigma_{ij}$. The two-body LJ parameters quantities are derived from one-body parameters using the conventional Lorentz-Berthelot combining rules: $R_{e,ij} = 1/2(R_{e,ii} + R_{e,jj})$ and $\sigma_{ij} = \sqrt{\sigma_{ii}\sigma_{jj}}$. The independent one-body LJ parameters ϵ_{ii} and $R_{e,ii}$ are listed in Table II, and were chosen to fit *ab initio* using an analogous procedure to that of the OPN model: the rare gas parameters were chosen from the homonuclear dimer potentials, and the F and Cl parameters were taken from the NeF and NeCl potentials, respectively.

As mentioned in Sec. II A, the present work considers the MNDO/d Hamiltonian, which was chosen because it provided a convenient and natural extension to our work in Ref. 86. We now briefly discuss this choice of semiempirical Hamiltonian as it relates to the model parameters. For the purposes of this work, it was our intent to examine small, *ad hoc* systems whose interactions were dominated by van der Waals forces. The interactions between atoms (or atomic ions) were chosen because these systems minimize the obfuscation of the results by the approximations inherent in the QM and MM Hamiltonians, i.e., the choice of these systems decreases the *coupling* of the QM/MM interaction energy to

TABLE II. Lennard-Jones parameters. All values in a.u. He, Ne, and Ar parameters were taken from the homonuclear rare gas potentials in Ref. 91. F and Cl parameters were determined from the NeF or NeCl *ab initio* potentials of this work.

	ϵ	R_e
He	3.3680E-5	5.624
Ne	1.3044E-4	5.856
Ar	4.4183E-4	7.140
F	2.7522E-4	5.282
Cl	4.9402E-4	6.935

TABLE III. Comparison of potential energy curves for He/Ne/Ar interactions using LJ and OPN models. Comparison of the dissociation energy (D_e) in mE_h , and energy minimum (R_e) and contact distance (σ) in angstrom, for the LJ, OPN models. Deviations with respect to the reference values are shown on the line immediately below each line of data.

	HeHe			NeNe			ArAr		
	σ	R_e	D_e	σ	R_e	D_e	σ	R_e	D_e
LJ	2.65	2.98	0.03	2.76	3.10	0.13	3.37	3.78	0.44
	0.00	0.00	0.00	-0.01	0.00	0.00	-0.01	0.00	0.00
OPN	2.68	2.98	0.03	2.75	3.10	0.13	3.36	3.78	0.44
	0.03	0.00	0.00	-0.02	0.00	0.00	-0.01	0.00	0.00
Ref.	2.65	2.98	0.03	2.77	3.10	0.13	3.37	3.78	0.44
	HeNe			HeNe			NeAr		
	σ	R_e	D_e	σ	R_e	D_e	σ	R_e	D_e
LJ	2.71	3.04	0.07	3.01	3.38	0.12	3.06	3.44	0.24
	0.01	0.01	-0.00	-0.11	-0.12	0.03	-0.06	-0.05	0.03
OPN	2.72	3.04	0.06	3.12	3.50	0.09	3.18	3.56	0.17
	0.02	0.02	-0.00	-0.00	0.00	-0.00	0.06	0.07	-0.03
Ref.	2.70	3.03	0.07	3.12	3.49	0.09	3.12	3.49	0.21

the specific forms of the QM and MM Hamiltonians. Mathematically, this is evident from Eq. (6), which is formally independent of the QM and MM Hamiltonians. In practice, the parameters in Table I *do* depend on the underlying Hamiltonians, insofar as the dipole polarizability correction parameters $\Delta\alpha(0)$ and B are *corrections* to the underlying Hamiltonian. Minimal basis set methods yield no polarization response for He, Ne, Ar, F^- , and Cl^- , i.e., all orbitals are occupied, and therefore the same polarizability correction would be used for any minimal basis Hamiltonian. MNDO/d includes an additional set of d orbitals on Cl, and like a minimal basis description of neutral F, this predicts a *small* semiempirical polarizability for these cases.

C. Comparison of the LJ and OPN models for rare gas (He, Ne Ar) homo and heterodimer interactions

Table III compares key quantities derived from the rare gas homodimer and heterodimer potential energy curves resulting from the OPN and LJ models with the corresponding *ab initio* reference results. Figures of the potential energy surfaces are provided as supplementary material.¹⁰³ In summary, both the OPN and LJ models generally perform very well for the homodimers, which is not surprising since they were parametrized against the homodimer reference curves. It is noteworthy that the OPN model more closely reproduces the individual repulsive and dispersion components of the interaction energy than the LJ model. Parametrization of the LJ potential to reproduce the equilibrium separation and well depth has the consequence that, in some instances (most pronouncedly for Ar–Ar), the LJ potential yields an attractive long-range tail that is slightly too attractive. In the case of the heterodimers that were not used to derive any of the model parameters, the situation is sometimes different; the LJ model performs fairly well for the HeNe curve, but considerably more poorly for the HeAr and NeAr curves where the errors in the σ , R_e , and D_e values are -0.11 \AA , -0.12 \AA , and $0.03mE_h$, respectively, for HeAr and -0.06 \AA , -0.05 \AA , and $0.03mE_h$, respectively, for NeAr. The OPN model performs significantly better, having very close agreement for

the HeNe and HeAr curves, and more significant errors for the NeAr curve (errors in the R_e and D_e values are -0.06 \AA , 0.07 \AA , and $-0.03mE_h$, respectively). It should be emphasized that the energy values are all considerably small, less than $0.44mE_h$ (0.7 kcal/mol). Overall, the OPN model is more accurate for the heterodimers, and performs slightly worse for the NeAr potential, where the error is similar in magnitude (but opposite in sign) to that of the LJ model.

D. Comparison of the LJ, OPN, and OPNQ models for rare gas (He, Ne, Ar) interactions with halogen atoms and ions (F/F^- , Cl/Cl^-)

Tables IV and V compare key quantities derived from the potential energy curves for rare gas interactions with F/F^- and Cl/Cl^- , respectively. In the case of the rare gas interacting with neutral F and Cl, results are similar between the LJ and OPN models. Both models perform well for F and Cl interactions with Ne, for which the halogen parameters were optimized. The interactions with He are also quite good, with the LJ and OPN curves for HeF having similar errors in the σ , R_e , and D_e values of 0.1 \AA , 0.1 \AA , and $0.02 mE_h$, respectively. The corresponding errors for HeCl are much lower. The largest error by far is for the ArF and ArCl curves where both the LJ and OPN models perform considerably more poorly. Both the LJ and OPN models are underbound, having errors in the D_e values for ArF of -0.13 and $-0.16 mE_h$, respectively, and for ArCl of -0.35 and $-0.10 mE_h$, respectively. The origin of the underbinding derives mainly from an outward shift in the contact distances from the *ab initio* values of 2.71 and 3.03 \AA for ArF and ArCl, respectively, to the LJ values of 2.93 and 3.32 \AA , respectively, and OPN values of 2.93 and 3.15 \AA , respectively. Alternately stated, the LJ and OPN models are more repulsive than the *ab initio* reference. Here, it is possible that the combining rules used in the models are perhaps not optimal, or alternately that there is a systematic difference in the reference potentials involving Ar. In any event, although the relative errors are considerable, their overall magnitude of the errors is still fairly small, less than 0.6 kcal/mol . When

TABLE IV. Comparison of potential energy curves for He/Ne/Ar interactions with F/F⁻ using LJ, OPN, and OPNQ models. Comparison of the dissociation energy (D_e) in mE_h , and energy minimum (R_e), and contact distance (σ) in angstroms, for the LJ, OPN, and OPNQ models. Deviations with respect to the reference values are shown on the line immediately below each line of data.

	HeF			NeF			ArF		
	σ	R_e	D_e	σ	R_e	D_e	σ	R_e	D_e
LJ	2.57	2.89	0.10	2.63	2.95	0.19	2.93	3.29	0.35
	0.10	0.09	-0.02	0.02	0.00	0.00	0.22	0.21	-0.13
OPN	2.57	2.90	0.09	2.60	2.95	0.19	2.93	3.31	0.32
	0.10	0.10	-0.02	-0.01	0.00	0.00	0.22	0.24	-0.16
Ref.	2.47	2.80	0.11	2.61	2.95	0.19	2.71	3.08	0.48
	HeF ⁻			NeF ⁻			ArF ⁻		
LJ	2.12	2.42	1.32	2.18	2.49	2.35	2.34	2.67	6.91
	-0.63	-0.86	1.01	-0.49	-0.65	1.54	-0.19	-0.35	2.97
OPN	1.97	2.33	1.40	2.04	2.40	2.54	2.09	2.51	7.74
	-0.79	-0.95	1.09	-0.64	-0.74	1.72	-0.45	-0.52	3.80
OPNQ	2.60	3.07	0.46	2.70	3.17	0.82	2.59	3.08	3.53
	-0.15	-0.21	0.15	0.03	0.03	0.00	0.05	0.06	-0.41
Ref.	2.75	3.28	0.31	2.67	3.13	0.82	2.54	3.02	3.94

charged systems are involved, the interaction energies are considerably larger, and ion-induced dipole terms dominate.

In the case of the rare gas interactions with charged F⁻ (Fig. 3) and Cl⁻ (Fig. 4) anions, the LJ and OPN are similar to one another, and exceedingly poor, whereas the OPNQ results are in very good agreement with the *ab initio* results. Both the LJ and OPN models are highly overbound. This is due to the fact that the contact distance is underestimated for rare gas interactions with the halogen anions, despite having been somewhat overestimated for the interactions with the neutral halogen atoms. In short, the repulsive potentials in the LJ and OPN models *do not change* with charge state, and hence the atomic size also does not change. This causes a severe underestimation of the repulsion due to the larger anions, and a corresponding overbinding of the rare gas-halide dimers. In the case of the LJ model, the error in the σ and D_e

values for F⁻ range from -0.19 to -0.63 Å and 1.01 to 2.97 mE_h , respectively, and for Cl⁻ range from -0.29 to -0.81 Å and 0.51 to 1.37 mE_h , respectively. The situation is even worse for the OPN model. When charge dependence is considered with the OPNQ model, however, the situation greatly improves. In the case of the rare gas interactions with the F⁻ anion (Fig. 3), the error in the σ values are -0.15, 0.03, and 0.05 Å for interactions with He, Ne, and Ar, respectively, and the corresponding error in the D_e values are 0.15, 0.00, and -0.41 mE_h , respectively. Similar results are observed for the rare gas interactions with the Cl⁻ anion (Fig. 4). In both cases, the biggest errors in σ occur for interactions with He, and the biggest errors in D_e occur for interactions with Ar. Overall, the improvement with the OPNQ model is striking, and demonstrates the need for inclusion of charge-dependent repulsion terms in

TABLE V. Comparison of potential energy curves for He/Ne/Ar interactions with Cl/Cl⁻ using LJ, OPN, and OPNQ models. Comparison of the dissociation energy (D_e) in mE_h , and energy minimum (R_e) and contact distance (σ) in angstroms, for the LJ, OPN, and OPNQ models. Deviations with respect to the reference values are shown on the line immediately below each line of data.

	HeCl			NeCl			ArCl		
	σ	R_e	D_e	σ	R_e	D_e	σ	R_e	D_e
LJ	2.96	3.32	0.13	3.02	3.39	0.25	3.32	3.72	0.47
	0.01	-0.01	0.00	0.01	0.00	0.00	0.29	0.29	-0.35
OPN	2.95	3.33	0.13	3.02	3.39	0.25	3.15	3.56	0.71
	0.00	0.00	0.01	0.01	0.00	0.00	0.12	0.13	-0.10
Ref.	2.95	3.33	0.13	3.01	3.39	0.25	3.03	3.43	0.81
	HeCl ⁻			NeCl ⁻			ArCl ⁻		
LJ	2.62	2.98	0.70	2.69	3.05	1.28	2.85	3.25	3.68
	-0.81	-1.03	0.51	-0.55	-0.70	0.78	-0.29	-0.43	1.37
OPN	2.55	2.96	0.70	2.63	3.04	1.27	2.65	3.10	4.47
	-0.88	-1.04	0.52	-0.61	-0.71	0.77	-0.49	-0.58	2.17
OPNQ	3.20	3.72	0.29	3.31	3.83	0.51	3.13	3.66	2.45
	-0.23	-0.29	0.10	0.07	0.07	0.01	-0.01	-0.02	0.15
Ref.	3.43	4.01	0.18	3.24	3.75	0.50	3.14	3.68	2.30

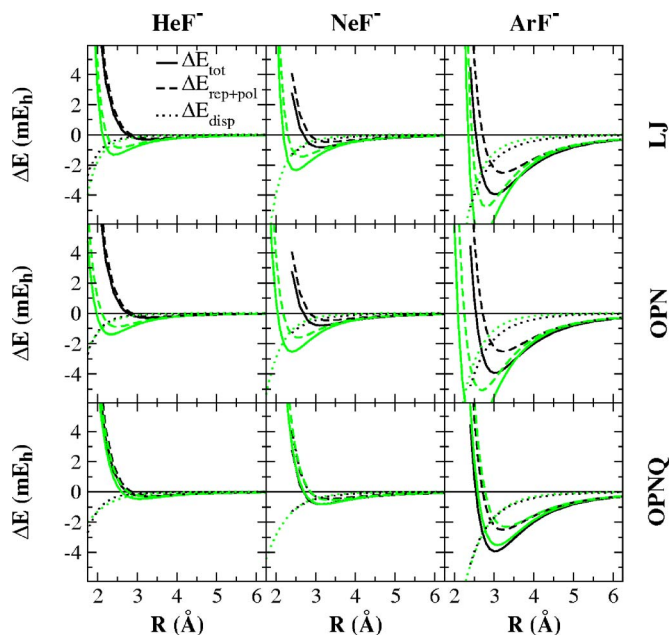


FIG. 3. (Color online) Comparison between the Lennard-Jones (LJ, top row), the charge-independent (OPN, middle row), and charge-dependent (OPNQ, bottom row) models described in the text, and *ab initio* Rg-F⁻ potential energy surfaces. The model and *ab initio* surfaces are shown in green and black, respectively. $\Delta E_{\text{rep+pol}}$ (dashed lines) is the sum of polarization and van der Waals repulsion energies. For OPN and OPNQ, this is the sum of E_{CPE} [Eq. (9)] and E_{rep} [Eq. (16)]. For LJ, this is the sum of E_{CPE} [Eq. (9)] and E_{LJ} [Eq. (42)]. The *ab initio* $\Delta E_{\text{rep+pol}}$ is the ΔE_{HF} data described in Sec. II D. ΔE_{disp} (dotted lines) is the van der Waals dispersion energy. For OPN and OPNQ, this is E_{disp} [Eq. (21)]. For LJ, this is $E_{\text{disp,LJ}}$ [Eq. (43)]. The *ab initio* ΔE_{disp} is the post-HF energy described in Sec. II D. ΔE_{tot} (solid lines) are the sum of $\Delta E_{\text{rep+pol}}$ and ΔE_{disp} .

QM/MM simulations where charge state can change considerably along the reaction coordinate, and modify significantly the exchange repulsion energy, and as a consequence

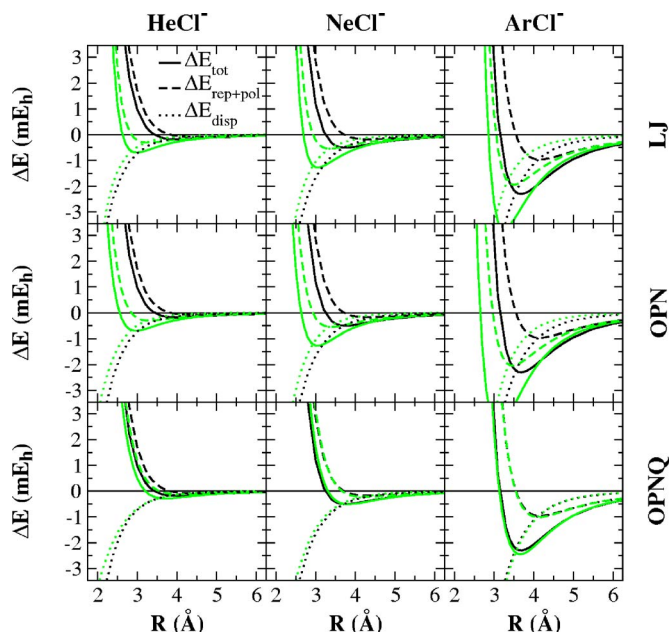


FIG. 4. (Color online) Comparison between the Lennard-Jones (LJ), the charge-dependent (OPNQ), and charge-independent (OPN) models described in the text, and *ab initio* Rg-Cl⁻ potential energy surfaces. See the caption of Fig. 3.

the degree of stabilization provided by the surrounding environment through coupled electrostatic and polarization terms.

IV. CONCLUSION

The present study develops a new charge-dependent model for many-body exchange and dispersion interactions that are coupled with polarization in a physically meaningful way with minimal parameters. As negative charge increases, the atomic size, softness, polarizability, and dispersion interactions also properly increase. The exchange repulsion is based on a simple scaled overlap model, motivated by a large set of data on rare gas homodimers and heterodimers. The model is tested against new benchmark *ab initio* results for rare-gas interactions with halogen atoms and halide anions (F/F⁻ and Cl/Cl⁻) which are also presented. Results indicate that the new model, for neutral atoms, is similar to the standard Lennard-Jones model, but offers tremendous improvement when variation in charge state is considered. The model is likely to be extremely important for improvement of next-generation QM/MM models where the local charge state of intermediates can undergo large variations along the reaction coordinate, requiring a smoothly varying description of differential exchange repulsion and polarization. It is the hope that this model will offer improved accuracy and robustness in these simulations, and obviate the need for tedious parametrization to specific “atom types” that can be ambiguous in QM/MM simulations.

ACKNOWLEDGMENTS

One of the authors (D.Y.) is grateful for financial support provided by the National Institutes of Health (Grant No. GM62248), the University of Minnesota Biomedical Informatics and Computational Biology program. Computational resources were provided by the Minnesota Supercomputing Institute and the IBM Blue Gene at the On-Demand Center in Rochester, Minnesota.

- ¹A. Warshel and M. Levitt, *J. Mol. Biol.* **103**, 227 (1976).
- ²M. J. Field, P. A. Bash, and M. Karplus, *J. Comput. Chem.* **11**, 700 (1990).
- ³J. Gao, *Rev. Comput. Chem.* **7**, 119 (1995).
- ⁴M. Garcia-Viloca, J. Gao, M. Karplus, and D. G. Truhlar, *Science* **303**, 186 (2004).
- ⁵B. A. Gregersen, T. J. Giese, Y. Liu, E. Mayaan, K. Nam, K. Range, and D. M. York, *Modelling Molecular Structure and Reactivity in Biological Systems*, Proceedings of the WATOC 2005, edited by K. J. Naidoo, J. Brady, M. J. Field, J. Gao, and M. Hann, (Royal Society of Chemistry, Cambridge, 2006), pp. 181–192.
- ⁶B. A. Gregersen, X. Lopez, and D. M. York, *J. Am. Chem. Soc.* **125**, 7178 (2003).
- ⁷B. A. Gregersen, X. Lopez, and D. M. York, *J. Am. Chem. Soc.* **126**, 7504 (2004).
- ⁸J. Gao, S. Ma, D. Major, K. Nam, J. Pu, and D. Truhlar, *Chem. Rev. (Washington, D.C.)* **106**, 3188 (2006).
- ⁹T.-S. Lee, C. Silva-Lopez, M. Matrick, W. G. Scott, and D. M. York, *J. Chem. Theory Comput.* **3**, 325 (2007).
- ¹⁰D. Riccardi, P. Schaefer, and Q. Cui, *J. Phys. Chem. B* **109**, 17715 (2005).
- ¹¹J. H. Jensen, H. Li, A. D. Robertson, and P. A. Molina, *J. Phys. Chem. A* **109**, 6634 (2005).
- ¹²D. Major, D. M. York, and J. Gao, *J. Am. Chem. Soc.* **127**, 16374 (2005).
- ¹³T. D. Poulsen, M. Garcia-Viloca, J. Gao, and D. G. Truhlar, *J. Phys.*

- Chem. B **107**, 9567 (2003).
- ¹⁴ I. Tejero, M. Garcia-Viloca, A. González-Lafont, J. Lluch, and D. York, J. Phys. Chem. B **110**, 24708 (2006).
- ¹⁵ W. L. Jorgensen and J. Tirado-Rives, J. Comput. Chem. **26**, 1689 (2005).
- ¹⁶ Y. Zhang, H. Liu, and W. Yang, J. Chem. Phys. **112**, 3483 (2000).
- ¹⁷ Y. Mo and J. Gao, J. Phys. Chem. A **104**, 3012 (2000).
- ¹⁸ M. Štrajbl, G. Hong, and A. Warshel, J. Phys. Chem. B **106**, 13333 (2002).
- ¹⁹ M. Topf and W. G. Richards, J. Am. Chem. Soc. **126**, 14631 (2004).
- ²⁰ M. Klähn, S. Braun-Sand, E. Rosta, and A. Warshel, J. Phys. Chem. B **109**, 15645 (2005).
- ²¹ H. Hu, Z. Lu, and W. Yang, J. Chem. Theory Comput. **3**, 390 (2007).
- ²² W. Thiel, Adv. Chem. Phys. **93**, 703 (1996).
- ²³ T. Clark, J. Mol. Struct.: THEOCHEM **530**, 1 (2000).
- ²⁴ P. Winget, C. Selçuki, A. Horn, B. Martin, and T. Clark, Theor. Chem. Acc. **110**, 254 (2003).
- ²⁵ W. Thiel, in *Handbook of Molecular Physics and Quantum Chemistry*, edited by S. Wilson (Wiley, Chichester, 2003), Vol. 2, pp. 487–502.
- ²⁶ M. Kolb and W. Thiel, J. Comput. Chem. **14**, 775 (1993).
- ²⁷ W. Weber and W. Thiel, Theor. Chem. Acc. **103**, 495 (2000).
- ²⁸ M. P. Repasky, J. Chandrasekhar, and W. L. Jorgensen, J. Comput. Chem. **23**, 1601 (2002).
- ²⁹ I. Tubert-Brohman, C. R. W. Guimaraes, M. P. Repasky, and W. L. Jorgensen, J. Comput. Chem. **25**, 138 (2003).
- ³⁰ I. Tubert-Brohman, C. R. W. Guimarães, and W. L. Jorgensen, J. Chem. Theory Comput. **1**, 817 (2005).
- ³¹ M. Elstner, T. Frauenheim, E. Kaxiras, G. Seifert, and S. Suhai, Phys. Status Solidi B **217**, 357 (2000).
- ³² Q. Cui, M. Elstner, E. Kaxiras, T. Frauenheim, and M. Karplus, J. Phys. Chem. B **105**, 569 (2001).
- ³³ D. Riccardi, P. Schaefer, Y. Yang *et al.*, J. Phys. Chem. B **110**, 6458 (2006).
- ³⁴ K. W. Sattelmeyer, I. Tubert-Brohman, and W. L. Jorgensen, IEEE Trans. Evol. Comput. **2**, 413 (2006).
- ³⁵ X. Lopez and D. M. York, Theor. Chem. Acc. **109**, 149 (2003).
- ³⁶ E. C. Sherer, D. M. York, and C. J. Cramer, J. Comput. Chem. **24**, 57 (2003).
- ³⁷ T. J. Giese, E. C. Sherer, C. J. Cramer, and D. M. York, J. Chem. Theory Comput. **1**, 1275 (2005).
- ³⁸ K. Nam, Q. Cui, J. Gao, and D. M. York, J. Chem. Theory Comput. **3**, 486 (2007).
- ³⁹ P. L. Cummins and J. E. Gready, J. Comput. Chem. **19**, 977 (1998).
- ⁴⁰ M. S. Formanek, G. Li, X. Zhang, and Z. Cui, J. Theor. Comput. Chem. **1**, 53 (2002).
- ⁴¹ G. Li, X. Zhang, and Q. Cui, J. Phys. Chem. B **107**, 8643 (2003).
- ⁴² O. Acevedo and W. L. Jorgensen, J. Am. Chem. Soc. **127**, 8829 (2005).
- ⁴³ M. R. Reddy, U. C. Singh, and M. D. Erion, J. Comput. Chem. **28**, 491 (2007).
- ⁴⁴ A. Warshe and M. Karplus, J. Am. Chem. Soc. **96**, 5677 (1974).
- ⁴⁵ J. Gao, N. Li, and M. Freindorf, J. Am. Chem. Soc. **118**, 4912 (1996).
- ⁴⁶ T. Vreven and K. Morokuma, J. Chem. Phys. **113**, 2969 (2000).
- ⁴⁷ M. Wanko, M. Hoffmann, P. Strodel, A. Koslowski, W. Thiel, F. Neese, T. Frauenheim, and M. Elstner, J. Phys. Chem. B **109**, 3606 (2005).
- ⁴⁸ M. Elstner, Theor. Chem. Acc. **116**, 316 (2006).
- ⁴⁹ C. Alhambra, J. Gao, J. Corchado, J. Villà, and D. G. Truhlar, J. Am. Chem. Soc. **121**, 2253 (1999).
- ⁵⁰ M. Garcia-Viloca, C. Alhambra, D. G. Truhlar, and J. Gao, J. Comput. Chem. **24**, 177 (2003).
- ⁵¹ H. Lin, Y. Zhao, O. Tishchenko, and D. G. Truhlar, J. Chem. Theory Comput. **2**, 1237 (2006).
- ⁵² J.-Y. Fang and S. Hammes-Schiffer, J. Chem. Phys. **106**, 8442 (1997).
- ⁵³ J.-Y. Fang and S. Hammes-Schiffer, J. Chem. Phys. **107**, 8933 (1997).
- ⁵⁴ A. Soudackov and S. Hammes-Schiffer, J. Am. Chem. Soc. **121**, 10598 (1999).
- ⁵⁵ H. Decornez and S. Hammes-Schiffer, J. Phys. Chem. A **104**, 9370 (2000).
- ⁵⁶ S. P. Webb and S. Hammes-Schiffer, J. Chem. Phys. **113**, 5214 (2000).
- ⁵⁷ J. Gao, J. Comput. Chem. **18**, 1061 (1997).
- ⁵⁸ R. Rjamani, K. J. Naidoo, and J. Gao, J. Comput. Chem. **24**, 1775 (2003).
- ⁵⁹ K. Nam, J. Gao, and D. M. York, J. Chem. Theory Comput. **1**, 2 (2005).
- ⁶⁰ J. Khandogin, B. A. Gregersen, W. Thiel, and D. M. York, J. Phys. Chem. B **109**, 9799 (2005).
- ⁶¹ B. A. Gregersen, J. Khandogin, W. Thiel, and D. M. York, J. Phys. Chem. B **109**, 9810 (2005).
- ⁶² A. R. Dinner, X. Lopez, and M. Karplus, Theor. Chem. Acc. **109**, 118 (2003).
- ⁶³ B. A. Gregersen and D. M. York, J. Comput. Chem. **27**, 103 (2006).
- ⁶⁴ B. A. Gregersen and D. M. York, J. Phys. Chem. B **109**, 536 (2005).
- ⁶⁵ P. Schaefer, D. Riccardi, and Q. Cui, J. Chem. Phys. **123**, 014905 (2005).
- ⁶⁶ J. Gao, P. Amara, C. Alhambra, and M. J. Field, J. Phys. Chem. A **102**, 4714 (1998).
- ⁶⁷ Y. Zhang, T.-S. Lee, and W. Yang, J. Chem. Phys. **110**, 46 (1999).
- ⁶⁸ I. Antes and W. Thiel, J. Phys. Chem. A **103**, 9290 (1999).
- ⁶⁹ N. Reuter, A. Dejaegere, B. Maigret, and M. Karplus, J. Phys. Chem. A **104**, 1720 (2000).
- ⁷⁰ D. M. Phillip and R. A. Friesner, J. Comput. Chem. **20**, 1468 (1999).
- ⁷¹ M. S. Gordon, M. A. Freitag, P. Bandyopadhyay, J. H. Jensen, V. Kairys, and W. J. Stevens, J. Phys. Chem. A **105**, 293 (2001).
- ⁷² J. Z. Z. Ai, M. Gao, D. W. Zhang, and Y. Zhang, Chem. Phys. Lett. **394**, 4714 (1998).
- ⁷³ Y. Mei, D. Zhang, and J. Zhang, J. Phys. Chem. A **109**, 2 (2005).
- ⁷⁴ Y. Mei, C. Ji, and J. Z. H. Zhang, J. Chem. Phys. **125**, 094906 (2006).
- ⁷⁵ T. J. Giese and D. M. York, J. Chem. Phys. **120**, 9903 (2004).
- ⁷⁶ B. R. Brooks, R. E. Bruccoleri, B. D. Olafson, D. J. States, S. Swaminathan, and M. Karplus, J. Comput. Chem. **4**, 187 (1983).
- ⁷⁷ A. D. MacKerell, Jr., J. Comput. Chem. **25**, 1584 (2004).
- ⁷⁸ D. M. Perreault and E. V. Anslyn, Angew. Chem., Int. Ed. Engl. **36**, 432 (1997).
- ⁷⁹ M. Oivanen, S. Kuusela, and H. Lönnberg, Chem. Rev. (Washington, D.C.) **98**, 961 (1998).
- ⁸⁰ M. Klähn, E. Rosta, and A. Warshel, J. Am. Chem. Soc. **128**, 15310 (2006).
- ⁸¹ J. Gao and X. Xia, Science **258**, 631 (1992).
- ⁸² F. J. Luque, N. Reuter, A. Cartier, and M. F. Ruiz-López, J. Phys. Chem. A **104**, 10923 (2000).
- ⁸³ D. Riccardi, G. Li, and Q. Cui, J. Phys. Chem. B **108**, 6467 (2004).
- ⁸⁴ M. Freindorf, Y. Shao, T. R. Furlani, and J. Kong, J. Comput. Chem. **26**, 1270 (2005).
- ⁸⁵ W. Thiel and A. A. Voityuk, J. Phys. Chem. **100**, 616 (1996).
- ⁸⁶ T. J. Giese and D. M. York, J. Chem. Phys. **123**, 164108 (2005).
- ⁸⁷ D. M. York and W. Yang, J. Chem. Phys. **104**, 159 (1996).
- ⁸⁸ S. Kita, K. Noda, and H. Inouye, J. Chem. Phys. **64**, 3446 (1976).
- ⁸⁹ R. J. Wheatley and S. L. Price, Mol. Phys. **69**, 507 (1990).
- ⁹⁰ J. Piquemal, G. Cisneros, P. Reinhardt, N. Gresh, and T. A. Darden, J. Chem. Phys. **124**, 104101 (2006).
- ⁹¹ T. J. Giese, V. M. Audette, and D. M. York, J. Chem. Phys. **119**, 2618 (2003).
- ⁹² K. T. Tang and J. P. Toennies, J. Chem. Phys. **80**, 3726 (1984).
- ⁹³ R. Pellenq and D. Nicholson, Mol. Phys. **95**, 549 (1998).
- ⁹⁴ R. Pellenq and D. Nicholson, Mol. Phys. **96**, 1001 (1999).
- ⁹⁵ A. J. Thakker, J. Chem. Phys. **89**, 2092 (1988).
- ⁹⁶ K. T. Tang and J. P. Toennies, Surf. Sci. Lett. **279**, L203 (1992).
- ⁹⁷ U. Kleinekathöfer, K. T. Tang, J. P. Toennies, and C. L. Yiu, J. Chem. Phys. **107**, 9502 (1997).
- ⁹⁸ S. F. Boys and F. Bernardi, Mol. Phys. **19**, 553 (1970).
- ⁹⁹ R. A. Kendall, T. H. Dunning, Jr., and R. J. Harrison, J. Chem. Phys. **96**, 6796 (1992).
- ¹⁰⁰ D. E. Woon and T. H. Dunning, Jr., J. Chem. Phys. **98**, 1358 (1993).
- ¹⁰¹ Basis sets were obtained from the Extensible Computational Chemistry Environment Basis Set Database, Version 6/19/03, as developed and distributed by the Molecular Science Computing Facility, Environmental and Molecular Sciences Laboratory which is part of the Pacific Northwest Laboratory, P.O. Box 999, Richland, Washington 99352, U.S.A., and funded by the U.S. Department of Energy. The Pacific Northwest Laboratory is a multiprogram laboratory operated by Battelle Memorial Institute for the U.S. Department of Energy under Contract No. DE-AC06-76RLO 1830. Contact David Feller or Karen Schuchardt for further information.
- ¹⁰² D. E. Woon and T. H. Dunning, Jr., J. Chem. Phys. **101**, 8877 (1994).
- ¹⁰³ See EPAPS Document No. E-JCPSA6-127-025735 for further discussion. This document can be reached through a direct link in the online article's HTML reference section or via the EPAPS homepage (<http://www.aip.org/pubservs/epaps.html>).
- ¹⁰⁴ *CRC Handbook of Chemistry and Physics*, edited by D. R. Lide, 83rd ed. (CRC, Boca Raton FL, 2003).